Electrical Conductance at Directly Bonded Si/Si Interfaces in Dependence on Oxygen Concentration in Bonding Ambient

Author names:

Atsuhiro Inomata, Naoki Sano, and Katsuaki Tanabe*

Affiliation:

Department of Chemical Engineering, Kyoto University, Nishikyo, Kyoto 615-8510, Japan

Corresponding author:

*Email: tanabe@cheme.kyoto-u.ac.jp

Keywords:

Semiconductor; Wafer bonding; Surface; Interface; Electronics; Photonics; Device

Abstract

Direct semiconductor wafer bonding is a versatile fabrication scheme for high-performance optoelectronic devices. In the present study, the influence of oxygen concentration in the bonding ambient on the electrical conductance at directly bonded Si/Si interfaces is experimentally investigated in relation to interfacial oxidation. The interfacial electrical conductivity is observed higher for lower oxygen concentration at each bonding temperature in the range of 200 – 400 ℃. Ohmic contact characteristics are found attainable in the bonded interfaces by proper choice of bonding conditions. To support the electrical conductance trend, an x-ray photoelectron spectroscopy analysis confirms the extent of interfacial oxidation to be higher for lower oxygen concentration and higher bonding temperature. In addition, solar cell fabrication and operation with a current path through the bonded interface are demonstrated by using the bonding method in a low oxygen concentration ambient. The energy conversion efficiency of the bonded cell is observed comparable to that of an unbonded reference, to thus verify the suitability of the bonding scheme for device applications.

Introduction

Semiconductor wafer bonding is a versatile fabrication scheme used in a variety of applications in electronics and photonics [1–6]. Representative optoelectronic devices generated through wafer bonding include light-emitting diodes [7–9], lasers [10–12], optical modulators [13,14], photodetectors [15–17], and solar cells [18–20]. To date, semiconductor wafer bonding process is typically carried out in vacuum chambers in cleanrooms, which inevitably takes substantial running costs. In view of commercialization, it is important to ease the process conditions to reduce the cost. In this context, we previously conducted direct semiconductor wafer bonding in ambient air in a regular, noncleanroom environment by understanding the environmental influences on bonding characteristics [21]. It should be noted that direct wafer bonding, in contrast to bonding methods mediated by interfacial agents such as oxides [5,11,22], metals [7,23,24], and organic materials [25–27], is particularly sensitive to the bonding atmosphere. Nevertheless, to the best of our knowledge, the relationship between oxygen concentration in the bonding atmosphere and bonding outcome has not yet been investigated in detail. In the present study, we fundamentally investigate the influence of oxygen concentration in the bonding atmosphere on the interfacial electrical conductivity, one of the most important characteristics of bonds, to further deepen the fundamental technical knowledge for direct semiconductor wafer bonding.

Experimental Methods

For the bonding experiments, we used epi-ready-grade, single-side-polished *p*-type Si wafers (thickness: 280 μm, crystalline plane orientation: <100>, dopant: boron, doping

concentration: ~ 1×10^{19} cm^{-3}). We carried out the whole experimental processes of this study in a non-cleanroom, regular experimental room with a particle density of approximately 5 million m^{-3}, which we measured with a regular particle counter. The surface of the polished side of the Si wafer was first spin-coated with photoresist (3000 rpm, 1 min) for the purpose to protect the Si surface to be bonded from scratches and particulates during the process of being diced [21]. Subsequently, the photoresist-coated Si wafer was soft-baked at 100 °C for 10 min on a hotplate. The Si wafer was then diced into 0.64 and 1.0 cm^2 pieces. After being diced, the Si pieces were submerged in acetone for 5 min to remove the photoresist coating and to degrease the Si surfaces to be bonded. Immediately after the acetone submergence, the Si pieces were rinsed with deionized water. The Si pieces were subsequently subject to a wet hydrofluoric (HF) treatment (9% aq, 1 min) to remove the SiO_2 native oxide layer formed on the Si surfaces [21,28]. After the HF treatment, the Si pieces were not rinsed with water [21]. The surfaces of the polished sides of a 0.64-cm^2 Si piece and a 1.0-cm^2 Si piece were then contacted each other with their Si (011) edges being aligned. The combination of dissimilar sizes of Si pieces allows for handling the pair only by touching the larger piece, to prevent accidental debonding by shear stress caused by simultaneously touching the two pieces, before the establishment of firm bonding. The two Si pieces were then bonded under a uniaxial pressure of 0.1 MPa at various temperatures in the range of 100 – 400 °C in an electric furnace under nitrogen flow with various rates in the range of 0 – 3.0 L/min for 3 h. The heating and cooling rates were approximately 10 °C/min.

For electrical measurements, ohmic electrodes comprising a Au–Ge–Ni alloy layer (80:10:10 wt%) and a pure Au layer with thicknesses of 30 and 150 nm, respectively, were sequentially deposited via thermal evaporation on both of the outer surfaces of the bonded Si pieces. In this manner, Au/Au–Ge–Ni/Si contacts were formed and covered the entire Si surfaces of the bonded samples. We did not apply any annealing for the contacts to prevent

potential heating influences to the bonded interfacial characteristics. We then measured the current–voltage characteristics across the bonded interfaces.

Using the developed direct bonding technique, we fabricated a Si solar cell bonded to a Si wafer to demonstrate the applicability of our bonded semiconductor interface in optoelectronic devices. Si solar cells were prepared by thermal diffusion of phosphorus (10^{19} – 10^{20} cm^{-3}) into one side of the surface region of a double-side-polished epi-ready *p*-type Si <100> wafers doped with boron (doping concentration of ~ 1×10^{16} cm^{-3}). After the phosphorus thermal diffusion, the boron doping concentration on the other surface was increased to the level of 10^{19} – 10^{20} cm^{-3} by ion implantation, in order to provide a sufficient electrical conductance at the bonded interface. The *p*-type side of the Si solar cell wafer was bonded to a bare Si wafer (the same *p*-type Si wafer used for the above bonding investigation) under the same process conditions as those in the bonding investigation. A bonding temperature of 300 °C and a nitrogen flow rate of 1.5 L/min were employed, providing the highest conductivity according to the bonding investigation. A front grid contact on top of the Si cell and bottom contact on the back of the bare Si wafer were formed with the Au/Au–Ge–Ni metal material in the same manner as in the bonding investigation. It should be noted that, in this electrode configuration, the current passes through the bonded interface in the solar cell operation. Therefore, this solar cell fabrication and operation test is suitable to evaluate the validity of our bonding scheme for optoelectronic device applications. For comparison, we also prepared a pristine reference solar cell sample from the same Si solar cell wafer with the same top and bottom electrodes but standing alone, not bonded with a bare Si wafer. Through this performance comparison, the loss in the power conversion efficiency by the electrical resistance at the bonded interface can be estimated.

Results and Discussion

Prior to the bonding experiments, the relationship between the nitrogen flow rate and the oxygen concentration in the bonding furnace was calibrated. To measure the oxygen concentration in the calibration run, an oxygen monitor was installed in the furnace. In advance of the calibration run, the original ambient air in the furnace was purged by flowing nitrogen with a rate of 3.0 L/min for 5 min. Subsequently, the nitrogen flow rate was changed into the designated value, and the oxygen concentration in the furnace was measured at room temperature by the monitor 1 h later, as the steady-state concentration. Figure 1 presents the calibration result: the dependence of the oxygen concentration in the furnace (i.e., the bonding ambient) on the nitrogen flow rate. As naively expected, the oxygen concentration in the bonding furnace becomes lower as the nitrogen flow rate becomes higher. In the range of the nitrogen flow rate of 0 – 1.5 L/min, the oxygen concentration is observed to decrease nearly linearly to the flow rate, to eventually saturate at 0.8 % in the faster region. To reflect this result, nitrogen flow rates of 0, 0.5, 1.0, and 1.5 L/min were employed in the following bonding experiments. The corresponding oxygen concentrations in the bonding furnace are 21, 13, 5.8, and 0.8 %, respectively.

Figure 2 presents the current–voltage characteristics of the Si/Si interfaces bonded in the conditions of varied temperatures and nitrogen flow rates in the furnace. It should be noted that bonding did not form for the bonding temperature of 100 ºC. For the values of current density, the raw data of the measured current value was simply divided by the nominal bonding area of 0.64 cm^2, corresponding to the area of the smaller Si piece. Depending on the bonding condition, i.e., bonding temperature and oxygen concentration, some current–voltage curves are observed to be straight, which represents the ohmic contact character, and others being rectified, which is Schottky barrier-like character. The rectified, diode-like current–

voltage characteristics are presumably due to the existence of an insulating oxide layer, namely SiO_2, at the bonded interface. In Fig. 2, it is observed that for the highest nitrogen flow rate of 1.5 L/min, ohmic current–voltage characteristics, which is preferable in many device applications, are observed for all of the bonding temperatures. This result can be attributed to the low oxygen concentration in the bonding ambient, which sufficiently suppresses the oxide formation to secure highly conductive bonded interfaces. In fact, it is generally observed in Fig. 2 that the interfacial electrical conductivity, represented by the amplitude of slope of the current-voltage curves, becomes higher for higher nitrogen flow rate, which corresponds to lower oxygen concentration. In addition, it is observed that the interfacial electrical conductivity becomes higher for higher bonding temperature, although this trend is not as outstanding as the abovementioned dependence on oxygen concentration. Figure 3 summarizes the results presented in Fig. 2, as output parameter of the interfacial electrical conductivity, plotting the dependence of the interfacial electrical resistivity on the oxygen concentration in the bonding ambient for varied bonding temperature. It should be noted that the measured raw data of current–voltage characteristics, such as those in Fig. 2, include all series resistances through the bonded sample. Therefore, we independently determined the contact resistivities of the metal electrode/semiconductor interfaces using the transmission line method [29–31], and then determined the pure resistivity at the bonded interface by subtracting them from the inverse slope of the current–voltage curve at an applied bias voltage of 0 V, to be converted into the electrical resistivity data presented in Fig. 3. Another merit of this technical manner is that the finally obtained resistivity value contains no influence of the oxidation of the outer Si surfaces of the bonded piece during the bonding process, but solely reflects the characteristics of the bonded Si/Si interface. It is observed in Fig. 3 again that the interfacial electrical conductivity becomes higher for lower oxygen concentration in the bonding ambient. The effectiveness of the reduction of oxygen concentration in bonding ambient has thus been thus demonstrated. The interfacial electrical

resistivities for the samples bonded in the lowest oxygen concentration, 0.8 %, are observed to be about 0.2 $\Omega\cdot cm^2$ for all of the bonding temperatures, 200, 300, and 400 ºC. These resistivity values are slightly higher than those in the case of direct bonding in vacuum, about 0.1 $\Omega\cdot cm^2$ [32].

To clarify the correlation between the oxygen concentration in the bonding ambient and interfacial oxidation, to explicitly explain the abovementioned dependence of interfacial electrical conductance, we carried out an x-ray photoelectron spectroscopy analysis for delaminated Si surfaces after bonding. Typical x-ray photoelectron spectra are shown in Fig. 4, for the samples bonded at 200, 300, and 400 ºC under a nitrogen flow rate of 1.5 L/min. The plots present the binding energy region for the Si *2p* orbitals. A potential concern about the influence of the additional oxidation of the Si surface in ambient air before the x-ray photoelectron spectroscopy measurement after the delamination of the bonded Si/Si interface is dissolved as long as we observe a clear variation in the signal intensities of oxygen among the bonding conditions, i.e., the degree of oxidation during the bonding process is dominant over that in ambient air at room temperature, which is consequently negligible. It is clearly observed in Fig. 4 that the peak for SiO_2 becomes larger for higher bonding temperatures, while that for Si is relatively stable. As a parameter that represents the extent of interfacial oxidation, we employ the ratio of the peak area for SiO_2 to that for Si. Figure 5 summarizes the SiO_2/Si peak ratio in x-ray photoelectron spectroscopy for all of the bonding conditions with varied bonding temperatures and oxygen concentrations. As observed, the intensity of the SiO_2 peak for the bonding temperature of 200 ºC lie below the detection limit of our x-ray photoelectron spectroscopy, for all of the oxygen concentrations. Presumably, the effect of the HF surface pretreatment to substantially suppress the interfacial oxidation may be retained at such a relatively low bonding temperature. Whilst, the SiO_2 peaks were clearly detected for the bonding temperatures above 300 ºC. Overall, it is generally observed that the degree of

interfacial oxidation is higher for higher oxygen concentration and bonding temperature.

Finally, we demonstrate a fabrication and operation of a solar cell device by using our bonding method. The solar cell structure has an electrical current path through the bonded Si/Si interface, and therefore this experiment is a proper testimony for device applications. The bonded interface securely survived during the fabrication process, thus demonstrating its mechanical stability. Figure 6 presents the light current–voltage characteristics of the fabricated Si solar cell via Si/Si bonding at 300 ºC with an oxygen concentration of 0.8 %, under an *Air Mass 1.5 Global*, 1-sun illumination (100 mW/cm^2). Also plotted in Fig. 6 is the light current–voltage curve of the unbonded reference Si solar cell. As observed, the light current–voltage characteristics of the bonded and unbonded cells are close to each other, which indicate that the bonded Si/Si interface does not degrade the solar cell performance and therefore is considered to be suitable for applications. The energy conversion efficiency of the bonded Si solar cell was measured as 6.1 %, which was observed highly comparable to the efficiency of 6.3 % for the unbonded reference cell. The interfacial electrical resistivity of about 0.2 $\Omega \cdot cm^2$ observed in Fig. 3 for the employed bonding condition (temperature: 300 ºC, oxygen concentration: 0.8 %) would in principle cause a voltage drop of about 4 mV for a current density of 20 mA/cm^2, i.e., less than 1 % reduction in the output voltage, and thus similarly in the conversion efficiency. Such a rough estimate for the influence of the electrical resistance at the bonded interface on the cell performance verifies the similarity in the conversion efficiency between the bonded and unbonded cells. The cause of the slightly larger short-circuit current observed for the bonded cell is unknown, but presumably being a matter of experimental error. We observed that by sufficiently suppressing the oxygen concentration in bonding ambient, the interfacial electrical resistivity in the bonded Si/Si interfaces can securely be well below 1 $ohm \cdot cm^2$, as presented in Fig. 3. It is generally thought that a series resistance below 1 $ohm \cdot cm^2$ does not significantly affect the overall light current-voltage

output performance for a 1-sun irradiation intensity [33,34]. The electrical characteristics of our bonding may thus be suitable, for instance, for the non-concentrator solar cell application.

Conclusions

In this study, we conducted a fundamental investigation on the influence of oxygen concentration in the bonding ambient on the electrical conductance at directly bonded Si/Si interfaces in relation to interfacial oxidation. The interfacial electrical conductivity was observed to be higher for lower oxygen concentration at each bonding temperature in the range of 200 – 400 ℃. Ohmic contact characteristics were found to be attainable in the bonded interfaces by proper choice of bonding conditions. To support the electrical conductance trend, we carried out a series of x-ray photoelectron spectroscopy analyses for the delaminated Si surfaces after bonding, to confirm that the extent of interfacial oxidation is higher for lower oxygen concentration and higher bonding temperature. Furthermore, solar cell fabrication and operation with a current pathway through the bonded interface were demonstrated by using the bonding method in reduced oxygen concentration. The energy conversion efficiency of the bonded cell was observed comparable to that of an unbonded reference, to thus verify the suitability of the bonding scheme for device applications.

Acknowledgments

This study was financially supported, in part, by the Iwatani Foundation and the Japan Society for the Promotion of Science (JSPS).

References

[1] J. B. Lasky, *Appl. Phys. Lett.* **48**, 78 (1986).

https://doi.org/10.1063/1.96768

[2] M. Shimbo, K. Furukawa, K. Fukuda, and K. Tanzawa, *J. Appl. Phys.* **60**, 2987 (1986).

https://doi.org/10.1063/1.337750

[3] Q.-Y. Tong, R. Gafiteanu, and U. Gösele, *J. Electrochem. Soc.* **139**, L101 (1992).

https://doi.org/10.1149/1.2069081

[4] S. Noda, K. Tomoda, N. Yamamoto, and A. Chutinan, *Science* **289**, 604 (2000).

https://doi.org/10.1126/science.289.5479.604

[5] G. K. Celler and S. Cristoloveanu, *J. Appl. Phys.* **93**, 4955 (2003).

https://doi.org/10.1063/1.1558223

[6] O. Moutanabbir, *ECS Trans.* **33**, 177 (2010).

https://doi.org/10.1149/1.3485617

[7] M. Ichikawa, T. Kemmochi, T. Mukai, M. Uomoto, and T. Shimatsu, *ECS J. Solid State Sci. Technol.* **9**, 015004 (2020).

https://doi.org/10.1149/2.0092001JSS

[8] S. Sinha, H.-A. Feng, C.-Y. Chung, C.-W. Tu, and R.-H. Horng, *ECS J. Solid State Sci.*

Technol. **9**, 015015 (2020).
https://doi.org/10.1149/2.0342001JSS

[9] K. Nishigaya and K. Tanabe, *ECS J. Solid State Sci. Technol.* **9**, 086002 (2020).
https://doi.org/10.1149/2162-8777/abb794

[10] J. Van Campenhout, P. Rojo-Romeo, P. Regreny, C. Seassal, D. Van Thourhout, S. Verstuyft, L. Di Cioccio, J. M. Fedeli, C. Lagahe, and R. Baets, *Opt. Express* **15**, 6744 (2007).
https://doi.org/10.1364/OE.15.006744

[11] K. Tanabe, M. Nomura, D. Guimard, S. Iwamoto, and Y. Arakawa, *Opt. Express* **17**, 7036 (2009).
https://doi.org/10.1364/OE.17.007036

[12] G. Crosnier, D. Sanchez, S. Bouchoule, P. Monnier, G. Beaudoin, I. Sagnes, R. Raj, and F. Raineri, *Nat. Photon.* **11**, 297 (2017).
https://doi.org/10.1038/nphoton.2017.56

[13] R. Takigawa, E. Higurashi, T. Suga, and T. Kawanishi, *Opt. Express* **19**, 15739 (2011).
https://doi.org/10.1364/OE.19.015739

[14] J.-H. Han, F. Boeuf, J. Fujikata, S. Takahashi, S. Takagi, and M. Takenaka, *Nat. Photon.* **11**, 486 (2017).
https://doi.org/10.1038/nphoton.2017.122

[15] H. Park, A. W. Fang, R. Jones, O. Cohen, O. Raday, M. N. Sysak, M. J. Paniccia, and J. E.

Bowers, *Opt. Express* **15**, 6044 (2007).
https://doi.org/10.1364/OE.15.006044

[16] L. Chen, P. Dong, and M. Lipson, *Opt. Express* **16**, 11513 (2008).
https://doi.org/10.1364/OE.16.011513

[17] D.-M. Geum, S. K. Kim, S. Lee, D. Lim, H.-J. Kim, C. H. Choi, and S.-H. Kim, *IEEE Electron. Dev. Lett.* **41**, 433 (2020).
https://doi.org/10.1109/LED.2020.2966986

[18] K. Tanabe, A. Fontcuberta i Morral, H. A. Atwater, D. J. Aiken, and M. W. Wanlass, *Appl. Phys. Lett.* **89**, 102106 (2006).
https://doi.org/10.1063/1.2347280

[19] K. Tanabe, K. Watanabe, and Y. Arakawa, *Sci. Rep.* **2**, 349 (2012).
https://doi.org/10.1038/srep00349

[20] F. Dimroth, T. N. D. Tibbits, M. Niemeyer, F. Predan, P. Beutel, C. Karcher, E. Oliva, G. Siefer, D. Lackner, P. Fuß-Kailuweit, A. W. Bett, R. Krause, C. Drazek, E. Guiot, J. Wasselin, A. Tauzin, and T. Signamarcheix, *IEEE J. Photovolt.* **6**, 343 (2016).
https://doi.org/10.1109/JPHOTOV.2015.2501729

[21] R. Inoue, N. Takehara, T. Naito, and K. Tanabe, *ACS Appl. Electron. Mater.* **1**, 936 (2019).
https://doi.org/10.1021/acsaelm.9b00118

[22] T. Yamashita, S. Hirata, R. Inoue, K. Kishibe, and K. Tanabe, *Adv. Mater. Interfaces* **6**, 1900921 (2019).
https://doi.org/10.1002/admi.201900921

[23] S. Palit, J. Kirch, G. Tsvid, L. Mawst, T. Kuech, and N. M. Jokerst, *Opt. Lett.* **34**, 2802 (2009).
https://doi.org/10.1364/OL.34.002802

[24] T. Hishida, J. Liang, and N. Shigekawa, *Jpn. J. Appl. Phys.* **59**, SBBB04 (2020).
https://doi.org/10.7567/1347-4065/ab4c8a

[25] G. Krauter, A. Schumacher, U. Gösele, T. Jaworek, and G. Wegner, *Adv. Mater.* **9**, 417 (1997).
https://doi.org/10.1002/adma.19970090512

[26] P. P. Absil, J. V. Hryniewicz, B. E. Little, F. G. Johnson, K. J. Ritter, and P. T. Ho, *IEEE Photon. Technol. Lett.* **13**, 49 (2001).
https://doi.org/10.1109/68.903217

[27] J. Oberhammer, F. Niklaus, and G. Stemme, *Sensors Actuators A* **105**, 297 (2003).
https://doi.org/10.1016/S0924-4247(03)00202-4

[28] K. Ljungberg, Y. Bäcklund, A. Söderbärg, M. Bergh, M. O. Andersson, and S. Bengtsson, *J. Electrochem. Soc.* **142**, 1297 (1995).
https://doi.org/10.1149/1.2044167

[29] Y. Xu, R. Gwoziecki, I. Chartier, R. Coppard, F. Balestra, and G. Ghibaudo, *Appl. Phys. Lett.* **97**, 063302 (2010).
https://doi.org/10.1063/1.3479476

[30] S. Eidelloth and R. Brendel, *IEEE Electron Dev. Lett.* **35**, 9 (2014).
https://doi.org/10.1109/LED.2013.2290602

[31] M. Weis, K. Lee, D. Taguchi, T. Manaka, and M. Iwamoto, *Jpn. J. Appl. Phys.* **53**, 011601 (2014).
https://doi.org/10.7567/JJAP.53.011601

[32] J. Liang, L. Chai, S. Nishida, M. Morimoto, and N. Shigekawa, *Jpn. J. Appl. Phys.* **54**, 030211 (2015).
https://doi.org/10.7567/JJAP.54.030211

[33] P. R. Sharps, M. L. Timmons, J. S. Hills, and J. L. Gray, *Proc. 26th IEEE Photovolt. Specialists Conf.*, 895 (1997).
https://doi.org/10.1109/PVSC.1997.654231

[34] S. Yoshidomi, J. Furukawa, M. Hasumi, and T. Sameshima, *Energy Procedia* **60**, 116 (2014).
https://doi.org/10.1016/j.egypro.2014.12.352

Figure Captions

Fig. 1 Dependence of the oxygen concentration in the furnace (i.e., the bonding ambient) on the nitrogen flow rate.

Fig. 2 Current–voltage characteristics of the Si/Si interfaces bonded at (a) 200, (b) 300, and (c) 400 ℃, with varied nitrogen flow rate in the furnace.

Fig. 3 Dependence of the interfacial electrical resistivity on the oxygen concentration in the bonding ambient for varied bonding temperature.

Fig. 4 X-ray photoelectron spectra of the delaminated Si surface after bonding in an oxygen concentration of 0.8 % at varied temperatures.

Fig. 5 Dependence of the ratio of the SiO_2 peak area to the Si peak area in x-ray photoelectron spectroscopy on the oxygen concentration in the bonding ambient for varied bonding temperature.

Fig. 6 Light current–voltage characteristics of the bonded Si solar cell and the unbonded reference Si solar cell.

Figures

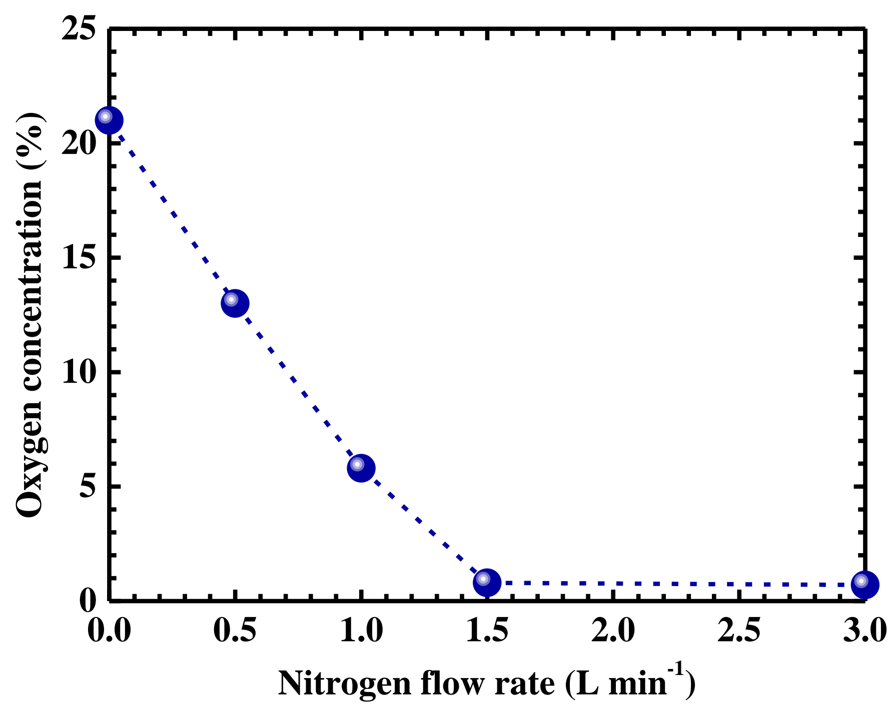

Fig. 1

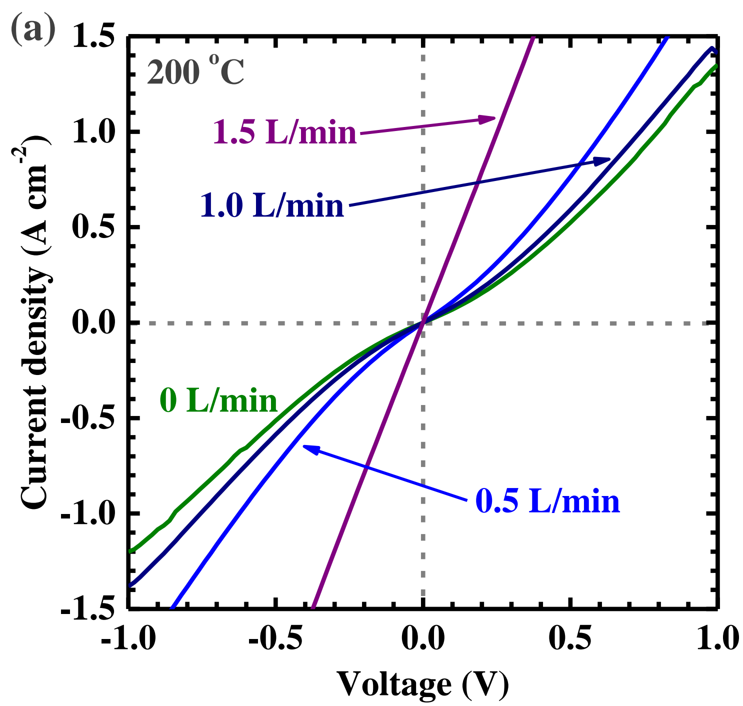

Fig. 2 (a)

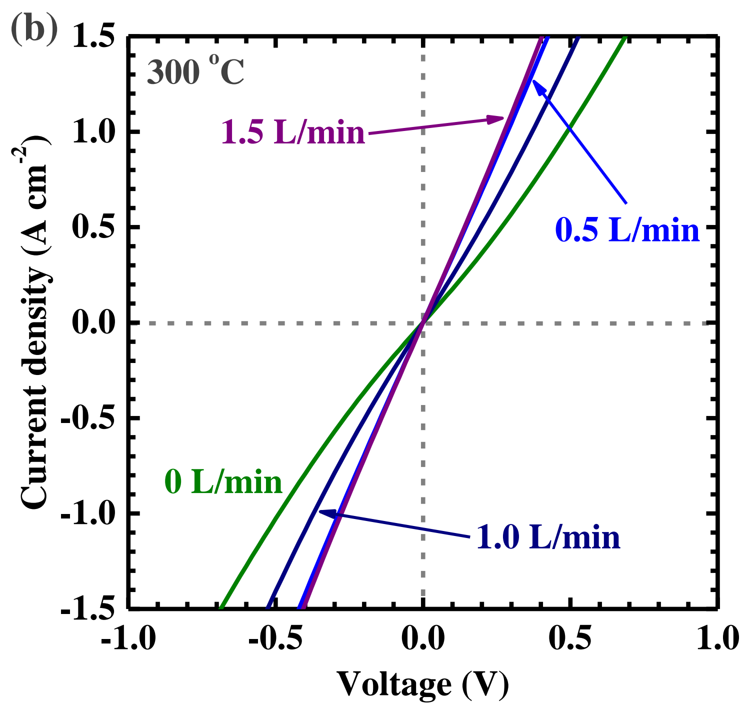

Fig. 2 (b)

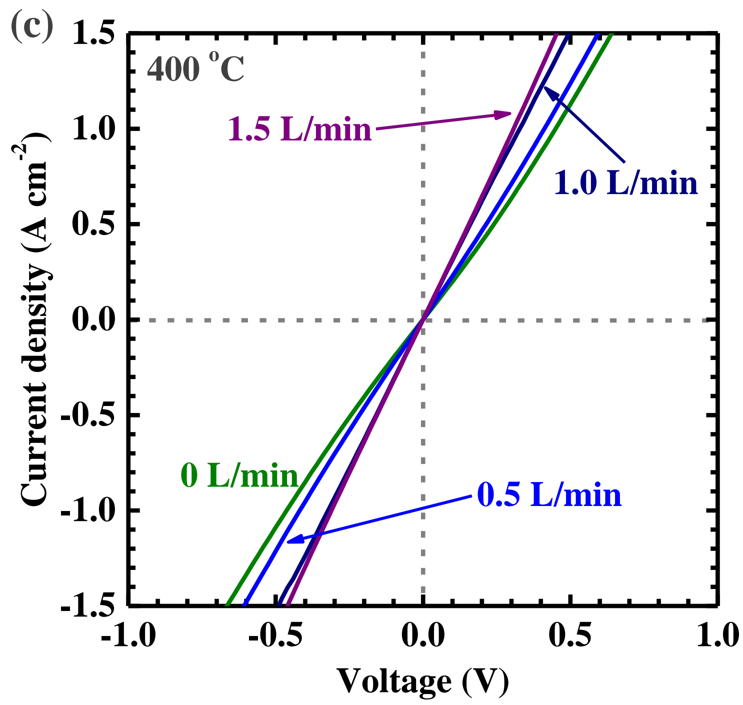

Fig. 2 (c)

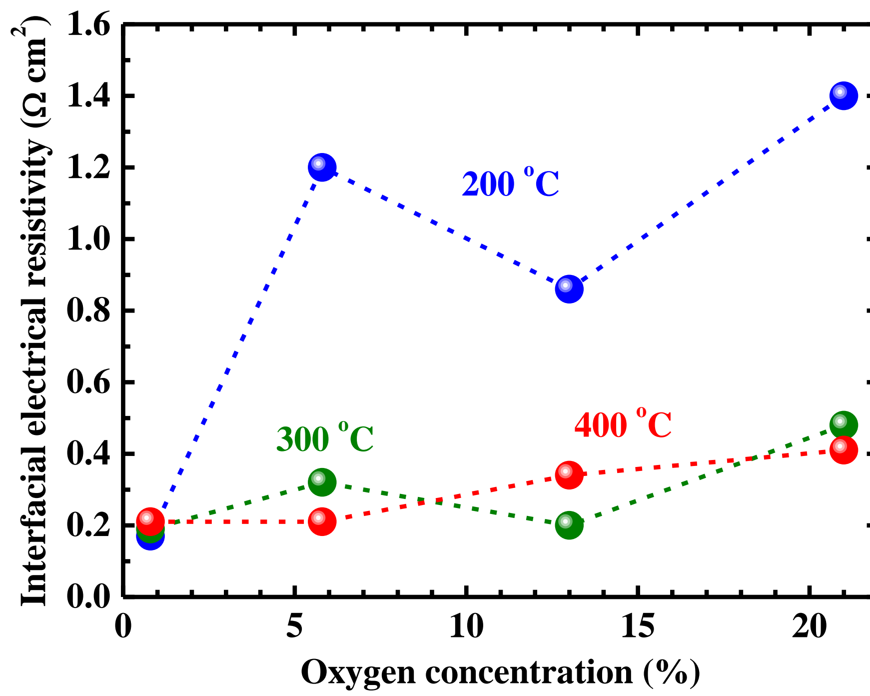

Fig. 3

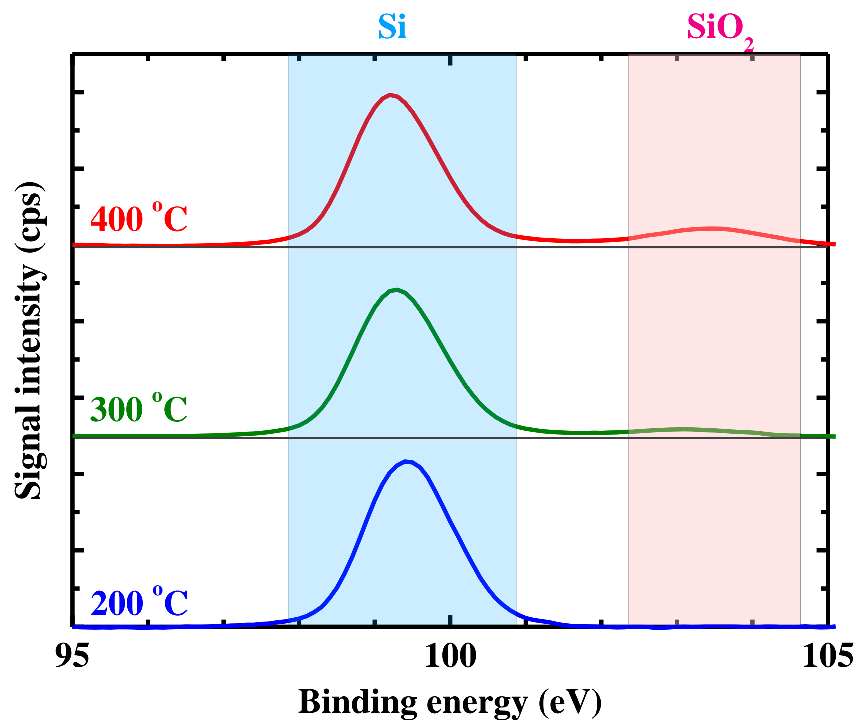

Fig. 4

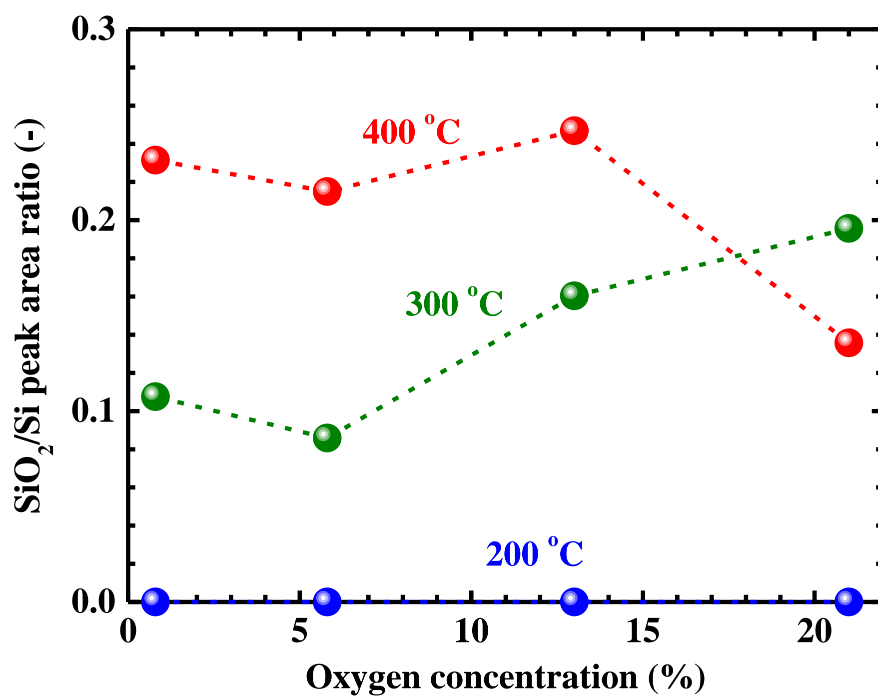

Fig. 5

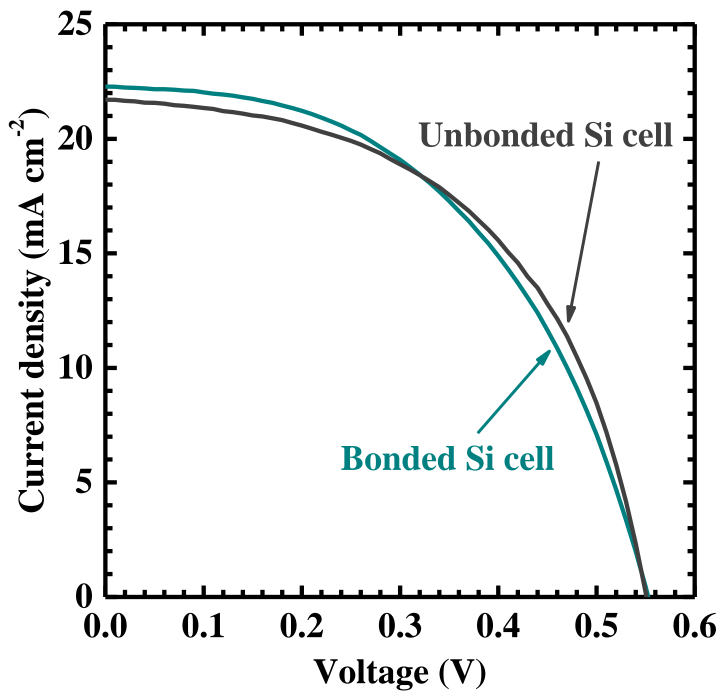

Fig. 6